2015

Methylmercury exposure during early Xenopus laevis development affects cell proliferation and death but not neural progenitor specification

Ryan W. Huyck
College of William and Mary

Maitreyi Nagarkar
College of William and Mary

Nina Olsen
College of William and Mary

Samuel E. Clamons
College of William and Mary

Margaret S. Saha
College of William and Mary

Recommended Citation

Huyck, R. W., Nagarkar, M., Olsen, N., Clamons, S. E., & Saha, M. S. (2015). Methylmercury exposure during early Xenopus laevis development affects cell proliferation and death but not neural progenitor specification. Neurotoxicology and teratology, 47, 102-113.

Neurotoxicology and Teratology 47 (2015) 102–113

Contents lists available at ScienceDirect

Neurotoxicology and Teratology

journal homepage: www.elsevier.com/locate/neutera

Methylmercury exposure during early *Xenopus laevis* development affects cell proliferation and death but not neural progenitor specification

Ryan W. Huyck [a], Maitreyi Nagarkar [b,1], Nina Olsen [b,2], Samuel E. Clamons [b,3], Margaret S. Saha [b,*]

[a] Department of Applied Science, College of William and Mary, McGlothlin-Street Hall, 251 Jamestown Road, Williamsburg, VA 23185, United States
[b] Department of Biology, College of William and Mary, Integrated Science Center, 540 Landrum Drive, Williamsburg, VA 23185, United States

ARTICLE INFO

Article history:
Received 26 July 2014
Received in revised form 25 November 2014
Accepted 27 November 2014
Available online 10 December 2014

Keywords:
Methylmercury
Xenopus
Neurodevelopment
Teratology
Toxicity

ABSTRACT

Methylmercury (MeHg) is a widespread environmental toxin that preferentially and adversely affects developing organisms. To investigate the impact of MeHg toxicity on the formation of the vertebrate nervous system at physiologically relevant concentrations, we designed a graded phenotype scale for evaluating *Xenopus laevis* embryos exposed to MeHg in solution. Embryos displayed a range of abnormalities in response to MeHg, particularly in brain development, which is influenced by both MeHg concentration and the number of embryos per ml of exposure solution. A TC_{50} of ~50 μg/l and LC_{50} of ~100 μg/l were found when maintaining embryos at a density of one per ml, and both increased with increasing embryo density. *In situ* hybridization and microarray analysis showed no significant change in expression of early neural patterning genes including *sox2*, *en2*, or *delta*; however a noticeable decrease was observed in the terminal neural differentiation genes *GAD* and *xGAT*, but not *xVGlut*. *PCNA*, a marker for proliferating cells, was negatively correlated with MeHg dose, with a significant reduction in cell number in the forebrain and spinal cord of exposed embryos by tadpole stages. Conversely, the number of apoptotic cells in neural regions detected by a TUNEL (terminal deoxynucleotidyl transferase dUTP nick end labeling) assay was significantly increased. These results provide evidence that disruption of embryonic neural development by MeHg may not be directly due to a loss of neural progenitor specification and gene transcription, but to a more general decrease in cell proliferation and increase in cell death throughout the developing nervous system.

1. Introduction

Generated by both natural and anthropogenic sources, mercury is a potent toxin for both humans and wildlife that has become a worldwide health concern (Mergler et al., 2007). Easily transported through the atmosphere due to its low boiling point, elemental mercury can be deposited far from its source where it rapidly enters the food chain through methylation by microorganisms into a highly bioavailable methylmercury (MeHg) form (Amyot et al., 2005; Harris et al., 2007; Schaefer et al., 2011). Because of MeHg's relatively long half-life in biological tissues, there is considerable biomagnification (Chumchal et al., 2011; Horvat et al., 2013), leading to elevated concentrations and increased toxicity in animals at higher trophic levels (Schmitt et al., 2011; Spada et al., 2012). On the biochemical level, toxicity is facilitated by the ability of MeHg to conjugate with the exposed thiol group of cysteine, leading to disruption of thiol and selenol rich enzyme activities (Carvalho et al. 2008; Zemolin et al., 2012) and providing MeHg active transport across the blood–brain and placental barriers through formation of a methionine mimic with free cysteine (Simmons-Willis et al., 2002; Yin et al., 2008).

Because of an observed elevated sensitivity in embryos, a number of studies have focused on examining the specific mechanisms underlying MeHg's effects on the developing nervous system at both the phenotypic and cellular molecular level (Patel and Reynolds, 2013). *In vivo* invertebrate studies with physiologically relevant exposures have shown a link between MeHg induced activation of the Notch pathway and a failure in proper neuron migration, survival, and axon outgrowth during *Drosophila* development (Rand et al., 2008, 2009; Engel et al., 2012; Engel and Rand, 2014). Embryological work using *Xenopus* at environmentally relevant concentrations of MeHg in solution found general toxicity beginning around 50 μg/l along with significant axial deformities and shortening of the embryo (Prati et al., 2002), disruption of metamorphosis independent of T3 levels (Davidson et al., 2011), and identified biomarkers strongly related to MeHg exposure (Monetti et al.,

* Corresponding author at: Department of Biology, Integrated Science Center 1, Landrum Drive, Williamsburg, VA 23185, United States. Tel.: +1 757 221 2407, +1 757 221 2212 (Lab); fax: +1 757 221 6483.
E-mail address: mssaha@wm.edu (M.S. Saha).
[1] Present address: Scripps Institution of Oceanography, 3120 Hubbs Hall, 8750 Biological Grade, La Jolla, CA 92093, United States.
[2] Present address: VCU School of Medicine, McGlothlin Medical Education Center, 1201 E Marshall Street, Richmond, VA 23298, United States.
[3] Present address: California Institute of Technology, 1200 East California Boulevard, Pasadena, CA 91125, United States.

http://dx.doi.org/10.1016/j.ntt.2014.11.010

2002). In rodents, many experiments involving human-like prenatal modes of exposure have examined the resulting behavioral and cognitive defects (for review see: Bisen-Hersh et al., 2014). A few rodent studies investigated developmental mechanisms of toxicity, noting aberrant neural cell migration (Guo et al., 2013), long lasting defects in the glutathione pathway (Stringari et al., 2008), and alterations in the expression of genes related to structural development of the brain in the cerebellum of both rats and mice (Padhi et al., 2008; Radonjic et al., 2013). However, the majority of these studies focus on developmental defects in the postnatal animal, and therefore cannot capture potential responses to toxicity occurring during the earliest phases of neurulation and gene patterning. Research in zebrafish has begun to address this by examining earlier time points in neurodevelopment, and has found a decrease in the proliferation of cells in the neural tube (Bertossi et al., 2004), along with disruption of genes related to oxidative stress and apoptosis (Yang et al., 2007; Ho et al., 2013).

While these results have given a clearer picture of the deleterious effect of MeHg on neurodevelopment, they are based on studies using a wide array of different model organisms with extremely varied dose and timing regimens, making direct comparisons difficult. In light of this, we have employed environmentally relevant concentrations of MeHg in a continuous exposure protocol using *Xenopus laevis* to advance our knowledge of early vertebrate developmental effects, such as neural patterning gene transcription, cell proliferation, and apoptosis at earlier developmental stages than previously done, and provide a comparison to studies conducted in zebrafish and other vertebrate model systems. In addition, to enhance our mechanistic understanding of embryonic toxicity, we have performed a time course assay of MeHg uptake to observe how this process changes with developmental stage, examined the effects of embryo density on toxicity response, and examined changes in early global transcription by microarray. The data from these experiments supports the hypothesis that failure of neuronal survival, rather than loss of neural patterning specification, may serve as a mechanism for MeHg toxicity during early neurodevelopment.

2. Methods

2.1. Animal care and embryo collection

All animal and embryo handling was conducted in accordance with the Institutional Animal Care and Use Committee guidelines at the College of William and Mary. *X. laevis* male and female frogs were injected with 250 and 700 units of human chorionic gonadotropin (Intervet), respectively, and up to a thousand embryos at a time were collected from one to two females in four batches from a single tray throughout the day. Embryos were dejellied for 3–5 min in a solution of 2% L-cysteine in 0.1× Marc's Modified Ringer (MMR) supplemented with 50 μg/ml gentamicin, pH 7.8 to 8.0. The 0.1× MMR was made through a serial dilution of 10× MMR (1 M NaCl, 20 mM KCl, 10 mM MgSO4, 20 mM $CaCl_2$, 50 mM HEPES, pH 7.4–7.6). After being dejellied, embryos were rinsed three times in 0.1× MMR to remove the remaining L-cysteine. Unfertilized eggs and otherwise deformed embryos were discarded within a few hours of collection. Embryos were staged according to Nieuwkoop and Faber (1994). Specifically of importance for this study are: the first cleavage stage 2 (1.5 h post fertilization (hpf)), cleavage stages 4–6 (2.25–3 hpf), blastula stage 8 (5 hpf), gastrulation stages 10–12 (9–13.25 hpf), the early neurulation and neural folds stages 14–15 (16.5–17.5 hpf), the late neurulation stages 18–20 (19.75–22.75 hpf), the tailbud stage 25 (27.5 hpf), the swimming tadpole stage 37 (53.5 hpf), and the pre-metamorphosis stage 45 (98 hpf).

2.2. Preparation of MeHg solutions

A stock of 10 mg/l MeHg solution was prepared by dissolving 12.5 mg of methylmercury chloride (MeHgCl) into 1 l of sterile double distilled (sdd) H_2O. The 10 mg/l stock was then diluted 1:10 with sdd H_2O, and total mercury content was quantitated using a Milestone Direct Mercury Analyzer-80 (DMA) before final dilutions in 0.1× MMR with gentamicin were made for working solutions. The working solutions prepared from the 1 mg/l solution include: 200 μg/l, 150 μg/l, 100 μg/l, 75 μg/l, 50 μg/l, and 10 μg/l, and were verified for mercury content by DMA (see Section 2.4) at the start of each exposure experiment.

2.3. Mercury exposure experiments

After removal of the jelly coat, embryos at the two-cell stage from the same batch were unbiasedly sorted into 35 mm, 60 mm, or 100 mm polystyrene Fisherbrand petri dishes containing either 5 ml, 10 ml, or 20 ml of medium, respectively, at recorded densities. The different dish sizes were selected to minimize embryo use according to the number of embryos needed for sufficient N at all doses for a particular experiment and subsequent downstream assays. The media for control groups was 0.1× MMR with gentamicin (DMA measured to contain 0.00 μg/l mercury). Sibling embryos from the same batch were exposed to a range of MeHgCl working solutions and control solution. Exposure began at the two-cell stage and embryos were kept in the same solution until the end of the experiment, constituting a one-time continuous dose of MeHgCl. Developmental progress was assessed using a graded 0–5 scale (Fig. 1) and the number of embryos for each phenotype was recorded at different stages. At the conclusion of the experiment, embryos were either fixed for *in situ* hybridization (ISH) in 1× MEMFA (100 mM MOPS

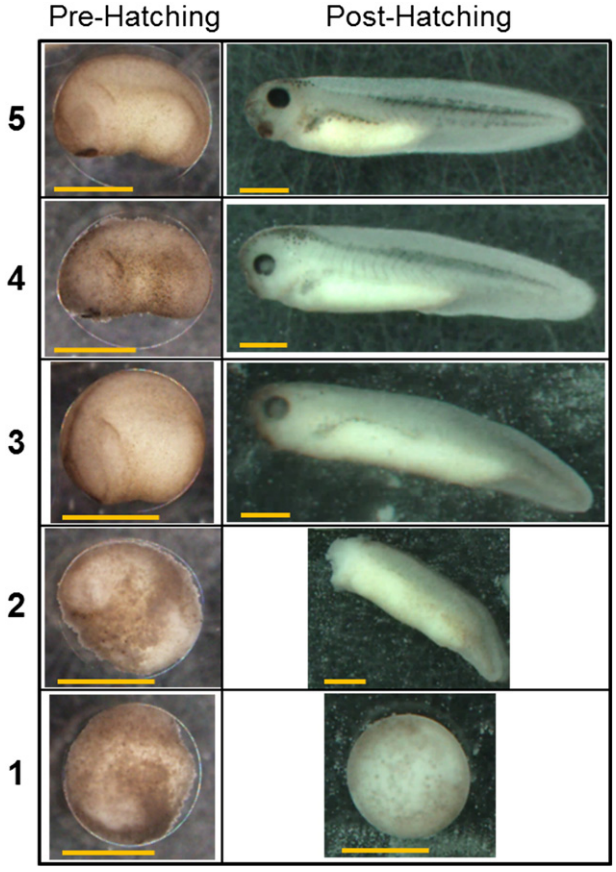

Fig. 1. Phenotype grading scale used for the visual analysis of the gross response of embryos to MeHg exposure. The scale applies to pre and post hatching embryos. The scores are: 5, normal development; 4, cell loss in vitelline membrane obscuring <25% of the embryo without gross deformity for pre-, or minor deformities with no loss of morphology, such as spine curling for post-; 3, two or more stages behind paired non-exposed controls; 2, large amount of cell loss to vitelline membrane obscuring >25% of embryo for pre-, or large amount of deformity causing loss of morphological features in post-; 1, ball of cells that has ceased to develop. Not shown is score 0, which is full lysis and removal. Scale bar represents 1 mm.

(pH 7.4), 2 mM EGTA, 1 mM $MgSO_4$, and 3.7% formaldehyde) for 90 min at room temperature (RT), or frozen for lyophilization and dry weight mercury content determination. Aliquots of the mercury solutions used for embryo exposure were taken both before and after exposure, and subsequently analyzed by DMA to assess uptake by the embryos.

2.4. Direct mercury analysis

Solution samples and freeze-dried embryos were analyzed by DMA in quartz boats and nickel boats, respectively, as previously published (Varian-Ramos et al., 2011), at a loading weight of ~0.02 g per sample. Duplicate DORM-4 and DOLT-4 (National Research Institute, Canada) reference standards were run for each load of 20 to 22 samples and an analytical run was performed if standards were within 7.5% of reference. Blanks were run before and after standards and sample runs. The DMA was calibrated every two months or as necessary using the above standards, and run according to the manufacturer's specifications.

2.5. ISH and TUNEL

A 1003 bp fragment of the *X. laevis* proliferating cell nuclear antigen (PCNA) gene (GenBank: NM_001087542) was cloned by RT-PCR (forward: 5′ – CGTCGCGGTAATCCCTTA – 3′; reverse: 5′ – TTGACCTCCT AGGGCAGAGA – 3′) from stage 40 *X. laevis* RNA into a pSC-A-amp/kan vector (Agilent). Antisense probe was made by linearizing the plasmid with XhoI and transcribing with T7 RNA polymerase. For Sox2, a 961 bp fragment of the *X. laevis* Sox2 gene (GenBank: AF022928) was cloned by RT-PCR (forward: 5′ – ATTCTGCCAGCCTTTGCTC – 3′; reverse: 5′ – CGTGCCATTGATCCCTGT – 3′) from stages 18–19 *X. laevis* RNA into a pCRII-TOPO vector (Life Technologies). Antisense probe was then made by EcoRV linearization and transcribed with Sp6 RNA polymerase. Delta was obtained in a pCMV-Sport6 vector from the IMAGE consortium (ID: 6636225; GenBank: BC070634), and antisense probe was produced by linearizing with EcoR1 and transcribing with T7 RNA polymerase. Engrailed-2 (En2) was obtained in the pBluescript vector from Addgene (plasmid 16950; Hemmati-Brivanlou et al., 1991; GenBank: NM_001101791), and antisense probe was made by linearizing with XbaI and transcribing with T3 RNA polymerase. Glutamic acid decarboxylase (GAD) (GenBank: U38225) and GABA transporter 1 (xGAT) (GenBank: AY904365) antisense probes were made as described by Li et al. (2006), while vesicular glutamate transporter 1 (xVGlut1) (GenBank: AF548627) antisense probe was made as described by Gleason et al. (2003). Sense probes were used as hybridization controls, and all probes were labeled with digoxygenin-rUTP (Roche). Whole mount ISH was carried out using a Biolane HTI following previously described methods (Harland, 1991), with minor modification, and visualized with BCIP/NBT color reaction. Embryos were then imaged with an Olympus SZH10 research stereoscope coupled with an Olympus DP71 digital camera.

Whole mount TUNEL was performed by permeabilizing embryos in phosphate buffer saline (PBS) with 0.1% Tween-20 five times for 15 min each, equilibrating for 1 h in terminal deoxynucleotidyl transferase (TdT; Sigma-Aldrich) buffer at RT, and incubating overnight at RT in TdT buffer with digoxigenin-dUTP (Roche) and 40 U of TdT enzyme (Sigma-Aldrich). The enzyme reaction was stopped by adding PBS with 100 mM EDTA and incubating at 65 °C two times for 30 min each. TUNEL positives were visualized by BCIP/NBT staining after labeling with alkaline phosphatase conjugated anti-digoxigenin antibody (Roche) 1:2000 overnight at 4 °C. Embryos were photographed with the same methods as the whole mount ISH.

2.6. Histology and cell counts

Histology was performed on ISH and TUNEL labeled embryos through cryosectioning or paraffin sectioning. For cryosectioning, embryos were first cryoprotected in 1.6 M sucrose in PBS for at least 12 h, embedded in Optimal Cutting Temperature media (Sakura) for at least 2 h, and then frozen at −20 °C. Following this, embryos were cryosectioned on a CryoStar NX70 microtome (Thermo Scientific) at a thickness of 18 μm and mounted on slides. For paraffin sectioning, embryos were dehydrated by gradated ethanol washes and cleared in 50% xylene/50% ethanol, followed by embedding in paraffin. Embryos were then sectioned by microtome at 10 μm thickness. After either method, slides were hydrated and equilibrated for 5 min in PBS, and stained for 15 min in 1× DAPI. Coverslips were then mounted on slides using Vectamount AQ (Vector Labs) or Fluoromount G (SouthernBiotech) for imaging on an Olympus BX60 microscope with an attached Media Cybernetics QCapture digital camera. Cell counts were performed using ImageJ. Regions of interest (ROI) capturing the neural tissue were selected from DAPI images of histological sections, and cells were automatically counted with the ITCN plugin (Byun et al., 2006) using a width of 6 pixels, minimal distance between nuclei of 3 pixels, and a peak threshold of 1.2. Counts of TUNEL positive cells were manually performed on the same ROIs using bright field images. Cell numbers from histological sections were averaged per brain region. Forebrain was defined as the neural regions up to the start of the eye, midbrain from beginning of the eye to the end of the eye, hindbrain from the end of the eye to the end of the otic vesicle, and spine being the remaining posterior sections.

2.7. qRT-PCR

Ten embryos from each exposure of 0, 75, and 150 μg/l MeHgCl were flash frozen in liquid nitrogen at stage 37. Embryos were subsequently homogenized while frozen by grinding with a pestle in 700 μl of TRIzol (Life Technologies). RNA was then extracted from the TRIzol homogenate using 4-bromoamisole and purified with an RNeasy Mini Kit (Qiagen), followed by cDNA synthesis with the iScript Reverse Transcription Supermix for RT-qPCR (Bio-Rad). qRT-PCR was performed with the Power SYBR Green PCR Master Mix (Applied Biosystems) on a StepOne Real-Time PCR System. The cycling program was: 95 °C for 10 min; then 40 cycles of 95 °C for 15 s and 60 °C for 1 min. Raw data was processed with the StepOne Software v2.3 by normalizing to the expression level of the reference gene, ornithine decarboxylase (ODC), and then again to the 0 μg/l control (ΔΔCT method), and subsequently analyzed in Microsoft Excel 2010 with the $2^{-\Delta\Delta C_T}$ method. Three technical replicates were performed for each gene and run. Primers used were: *PCNA* (forward: 5′ – CGTCAAGATGAGCAGTATGTC – 3′) and (reverse: 5′ – GATTTGGCGACTCAAACACC – 3′); and *ODC* (forward: 5′ – GCAAAGTGGATCTGATGATGAA – 3′) and (reverse: 5′ – CATCTGGT TTGGGTTTCTTTG – 3′).

2.8. Microarrays

Microarray analysis was performed with the Affymetrix GeneChip *Xenopus laevis* Genome 2.0 Array. The microarray was repeated for an N of 3, with each N consisting of the exposure of ten embryos to 0.0 μg/l and 200 μg/l MeHgCl, as described in Section 2.3 at a ratio of two embryos per ml (e/ml) of solution. Total RNA was extracted from each pool of ten embryos from the three independent experiments with the Qiagen RNeasy Mini Kit and sent to the Clemson University Genomics Institute. There, cDNA was produced from 500 ng total RNA using the 3′ IVT Express kit according to the manufacturer's instructions, except that the *in vitro* transcription reaction was carried out for 16 h. Hybridization, washing, staining, and scanning were performed according to the manufacturer's instructions. Raw data was normalized using Robust Microarray Average (RMA) (Irizarry et al., 2003) as implemented in the Bioconductor R (Gentleman et al., 2004) package. p-Values were calculated for each gene using the Limma package in Bioconductor R (Smyth, 2005) using a two-sample linear design model with group-means parameterization with Bayes correction. p-Values were corrected for multiple hypotheses testing by the Benjamini–Hochberg procedure

(Benjamini and Hochberg, 1995) and genes with significance of $p < 0.05$ after correction were considered differentially expressed (DE). Functional enrichment analysis on DE genes was performed in Partek Genomics Suite 6.6 using gene ontology (GO) enrichment and Partek Pathway, using the set of all genes in the Affymetrix CSV annotation for the *X. laevis* Genome 2.0 Array as of August 2010 (https://www.affymetrix.com/Auth/analysis/downloads/na31/ivt/X_laevis_2.na31.annot.csv.zip) as the background set.

2.9. Statistical analysis

Statistics were performed in Microsoft Excel 2010 using the Analysis ToolPak and Solver Add-in. Additional statistical functionality, was added to Excel by the Real Statistics Resource Pack v3.2.1 (Zaiontz, 2014). For testing differences in the distribution of embryos between phenotype ranks (Fig. 2), a two sample Kolmogorov–Smirnov test was used, with a Dunn–Sidak corrected $\alpha = 0.017$ for testing significant differences between total distributions of different embryo densities, and $\alpha = 0.0085$ for significance between doses within a particular density. For curve fitting to average phenotype data (Fig. 3a), a four parameter logistic curve of the form $y = D - ((A - D) / (1 - (x / C)^B))$ was fit using Excel's Solver Add-in set to minimize χ^2, with the values of 4.937 for A, 4.350 for B, 74.063 for C, and 0.958 for D, rounded to three significant figures. Concentrations of total mercury in embryo dry weight tissue across developmental stages (Fig. 3b) was analyzed by two factor ANOVA with replication followed by contrast analysis between particular MeHgCl doses with a Dunn–Sidak corrected $\alpha = 0.0102$. Finally, for comparisons between only two populations of data (Figs. 6i; 8i), a two tailed, unpaired Student's *t*-test was used.

3. Results

3.1. Morphological phenotype is dependent on dosage and density of the embryos

To assay the dose response of *X. laevis* embryos to MeHgCl, embryos were scored as described in Fig. 1. Dose response of embryos at the swimming tadpole stages 33–37 had a statistically significant dependence on the number of the embryos in a given volume of solution (hereafter referred to as density), determined by two sample Kolmogorov–Smirnov testing, with a $p = 1.16 * 10^{-5}$ for the distribution embryo rankings between 1 and 2 embryos per ml (e/ml) densities (Fig. 2a,b), a $p = 4.19 * 10^{-12}$ between 2 and 3 e/ml densities (Fig. 2b,c), and a $p = 1.08 * 10^{-7}$ between 1 and 3 e/ml densities (Fig. 2a,c). For embryos exposed to MeHg at a density of 1 e/ml, the teratogenic concentration at which 50% of embryos failed to develop normally (score < 5; TC_{50}) was ~50 μg/l MeHgCl (Fig. 2a). At a density of 2 e/ml, the TC_{50} was between 75 μg/l and 100 μg/l (Fig. 2b), and ~100 μg/l at 3 e/ml (Fig. 2c). These embryo densities resulted in a corresponding 50% lethal concentration (score ≤ 1; LC_{50}) of ~100 μg/l for 1 e/ml, between 100–150 μg/l for 2 e/ml, and ~200 μg/l for 3 e/ml. A significant difference in the distribution of embryo rankings was also observed for both 1 and 2 e/ml densities as early as between 0 and 50 μg/l ($p = 2.71 * 10^{-15}$ and $p = 1.76 * 10^{-7}$, respectively), but was not significant until between 0 and 100 μg/l for the 3 e/ml density ($p = 2.02 * 10^{-13}$).

Due to the dose responses' dependence on density, subsequent experiments were carried out at a 1 e/ml density, as this provided the widest variability in phenotypes within our range of solutions. Embryos displayed varying responses within the same plate, where a range of scores from 5 to 1 could be represented in a single experiment (Fig. 3c, *e.g.* 100 μg/l). However, the highest dose typically reached 100% lethality. The average phenotype score displayed a consistent decrease with increasing MeHgCl exposure (Fig. 3a), with an inflection point at 74 μg/l MeHgCl for the sigmoidal curve fit ($\chi^2 = 4.36$, $R^2 = 0.834$), which agrees with the phenotype distribution seen at 1 e/ml exposed to 75 μg/l MeHgCl (Fig. 2a).

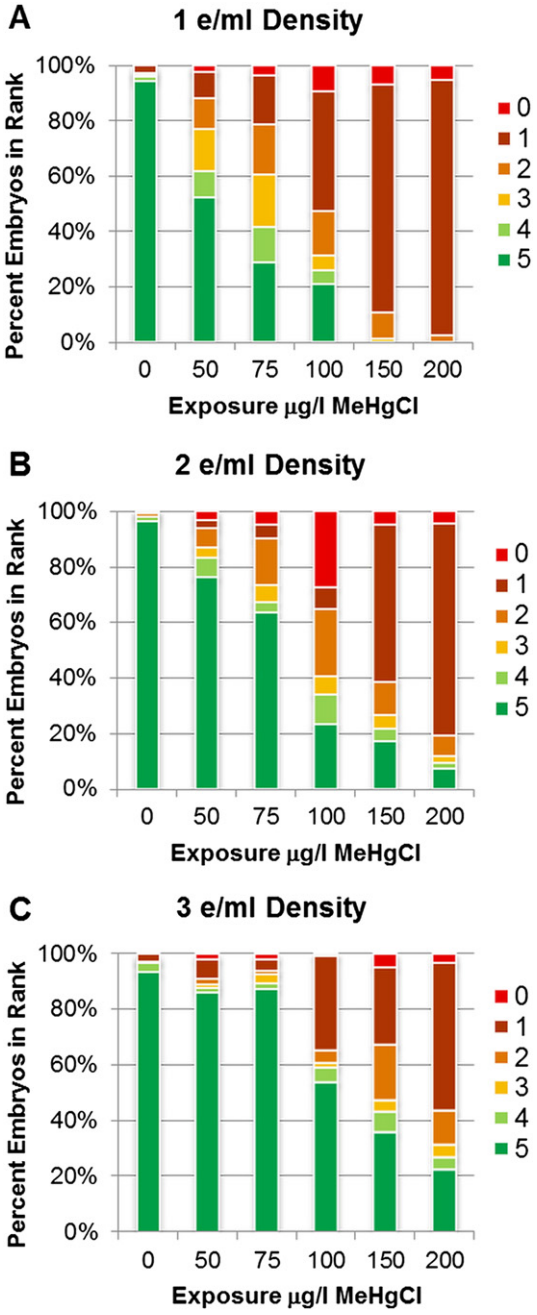

Fig. 2. Stacked percentages of embryos in each post hatching phenotype score at stage 33+ for a given exposure level of MeHgCl in solution. (A) Percentage of scores for embryos exposed at a density of 1 e/ml. N = 12 experiments, with 134 embryos total on average per dose. (B) and (C) are percentages of scores for embryo densities of 2 e/ml and 3 e/ml respectively. N = 17 experiments, with 320 embryos total on average; and N = 6 experiments, with 172 embryos total on average per dose, respectively.

Levels of total mercury detected in embryo dry weight tissue significantly increased with both increasing dose (N = 3 experiments, 15 embryos total per dose; two factor ANOVA: $F_{4,100} = 365.20$, $p = 1.03 * 10^{-58}$) as well as increasing developmental stage ($F_{9,100} = 82.61$, $p = 4.35 * 10^{-42}$) (Fig. 3b), with embryos ranging from an average of 64 ± 3.5 mg/kg at pre-metamorphosis stage 45 when exposed to 50 μg/l MeHgCl, to 110 ± 27.5 mg/kg from 200 μg/l exposure. There was also a significant interaction between stage and dose ($F_{36,100} = 10.9$, $p = 1.88 * 10^{-21}$) for the amount of detected mercury in tissue. The relative change in absorption between doses was less at intermediate concentrations, being statistically significant between 0 and 50 μg/l MeHgCl (ANOVA contrast: p = 0.0006), 50 and 100 μg/l (p = 0.0019),

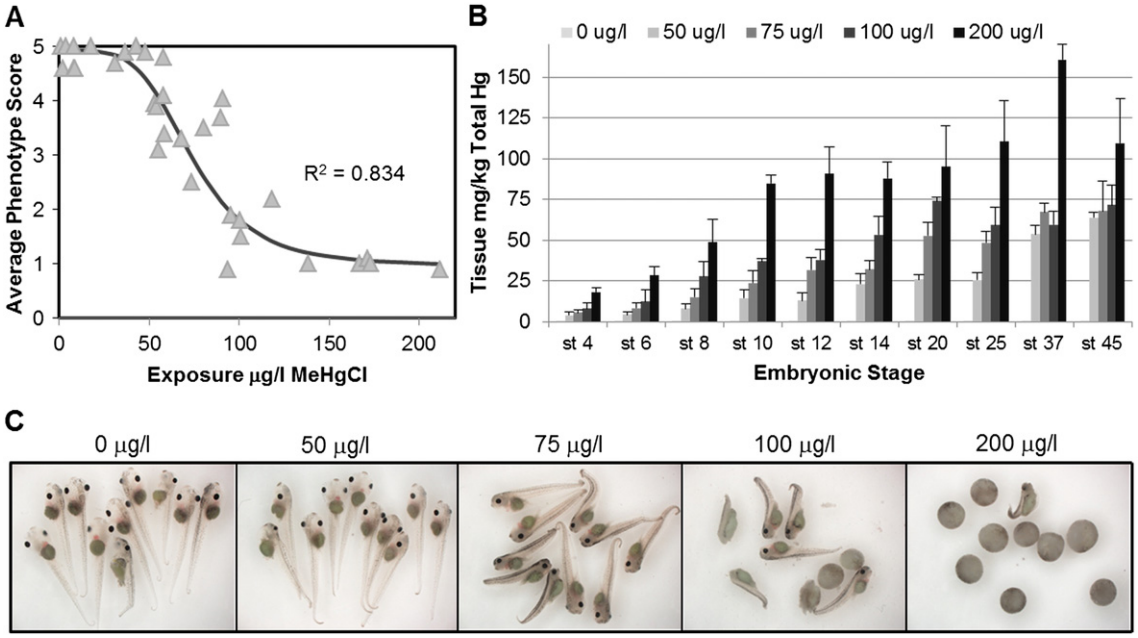

Fig. 3. Average response and MeHg uptake of embryos exposed to MeHgCl at a density of 1 e/ml. (A) Scatter plot of the average phenotype score of all embryos in an experiment by the starting concentration of MeHgCl in solution, as measured by DMA. Each triangle point represents one exposure experiment consisting of 10 to 20 embryos. A sigmoidal curve fit of $\chi^2 = 4.36$ is shown with its associated R^2. N = 32 experiments, with 370 embryos total. (B) Concentration of total Hg detected in embryo dry weight tissue per MeHgCl solution exposure at different embryonic stages as measured by DMA-80. N = 4 experiments, 20 embryos total per dose for stages 4–8 and 12, and 3 experiments and 15 embryos total per dose for stages 10 and 14–45. Error bars represent standard deviation. (C) Images of embryos at stages 45–46 exposed to indicated amounts of MeHgCl in solution. N = 12 experiments, with 138 total embryos on average per dose.

and 100 and 200 µg/l ($p = 2.49 * 10^{-8}$), but not significant between 50 and 75 µg/l ($p = 0.08$), or 75 and 100 µg/l ($p = 0.16$). Additionally, there was a significant difference after Dunn–Sidak multiple hypothesis correction ($\alpha = 0.01$) in the absorption of mercury by stage 4 between 0 and 200 µg/l MeHgCl ($p = 0.0004$), and between 0 and 50 µg/l by early gastrula stage 10 ($p = 0.006$).

Embryos exposed at a density of 2 e/ml displayed a similar MeHg uptake response by stage 37, but achieved burden values 42% less on average than stage 37 embryos at 1 e/ml above, while absorbing approximately 30% more MeHg from solution (N = 3 experiments, 15 embryos total per dose; data not shown), suggesting a partitioning of available MeHg between embryos driving the differences in MeHg uptake at the various embryonic densities. Additional experiments with MeHg pre-conjugated with cysteine (MeHgCys) at 1 e/ml using identical methods and exposures showed a much milder phenotypic effect, with 20% lethality at the 200 µg/l treatment level and a higher amount of non-deformed developmental delay (score 3) that peaked to ~50% with 100 µg/l MeHgCys (N = 3 experiments, 30 embryos total per dose; data not shown) compared to a ~20% peak at 75 µg/l MeHgCl. Despite this, embryos exposed to MeHgCys had the same level of mercury uptake into embryonic tissue as MeHgCl when measured by DMA (N = 2 experiments, 10 embryos total per dose; data not shown). Therefore, MeHgCl was chosen for continued experiments to allow analysis of developmental responses from 0% to 100% lethality within an environmental and physiological exposure range.

To determine temporal response to MeHg exposure, embryos were monitored over time. The percentage of experiments per developmental stage at which first signs of abnormalities were visible (a score < 5) was recorded (Table 1). No abnormalities in development were noticed at any dose up to stages 8–9, immediately prior to gastrulation, compared to controls. As the amount of MeHgCl increased, the percentage of experiments with embryo failure increased, and time of first deformity shifted to earlier stages. At the lowest concentrations of MeHgCl, 50 to 75 µg/l, developmental disruption was first seen at late neurula stages 18–20, with a larger fraction of experiments showing abnormalities in the 75 µg/l treatment group. At higher doses of MeHgCl, starting at 100 µg/l, deformities began to occur during the gastrulation stages 10–12, and by late neurula for exposures above 100 µg/l all experiments had embryos with disrupted phenotypes.

3.2. Early neural genes are unchanged while late neural phenotype markers are reduced by MeHg

To analyze the effects of MeHg exposure on the expression of early neural specific genes during development, ISH was performed on gastrula stages 11–12 and tailbud stages 23–24 embryos to probe for the expression patterns of the neural progenitor gene, *sox2*, the midbrain–hindbrain boundary marker, *en2*, and the Notch ligand, *delta*. The expression of both *sox2* and *en2* did not show differences in patterning at stages 11–12 (Fig. 4j–m) or 23–24 (Fig. 4a–f) for surviving embryos. Similarly, *delta* did not show abnormal expression (Fig. 4g–i and n–q), even at 100 µg/l MeHgCl.

For later neural gene expression, the excitatory neuron marker *xVGlut*, and the inhibitory neuron markers, *GAD* and *xGAT*, were investigated. While *xVGlut* did not display a discernible qualitative decrease in expression strength until the highest dose for half of embryos examined (Fig. 4u), barring cases where the head region failed to develop, there

Table 1
Stages where embryo development becomes disrupted by MeHgCl solution (score < 5).

MeHgCl	Stages 8–9	Stages 10–12	Stages 13–17	Stages 18–20	Stages 20–29	Stage 30+
50 µg/l	−	−	−	+	+	++
75 µg/l	−	−	−	+++	++++	++++
100 µg/l	−	++	++	+++	+++	++++
150 µg/l	−	++	++++	++++	++++	++++
200 µg/l	−	++	++	++++	++++	++++

Symbols indicate number of experiments where embryo deformity was observed at that dose: −, no experiments; +, >25% of experiments; ++, >50% of experiments; +++, >75% of experiments; ++++, 100% of experiments.
N = 6 experiments, and 70 embryos per stage on average.

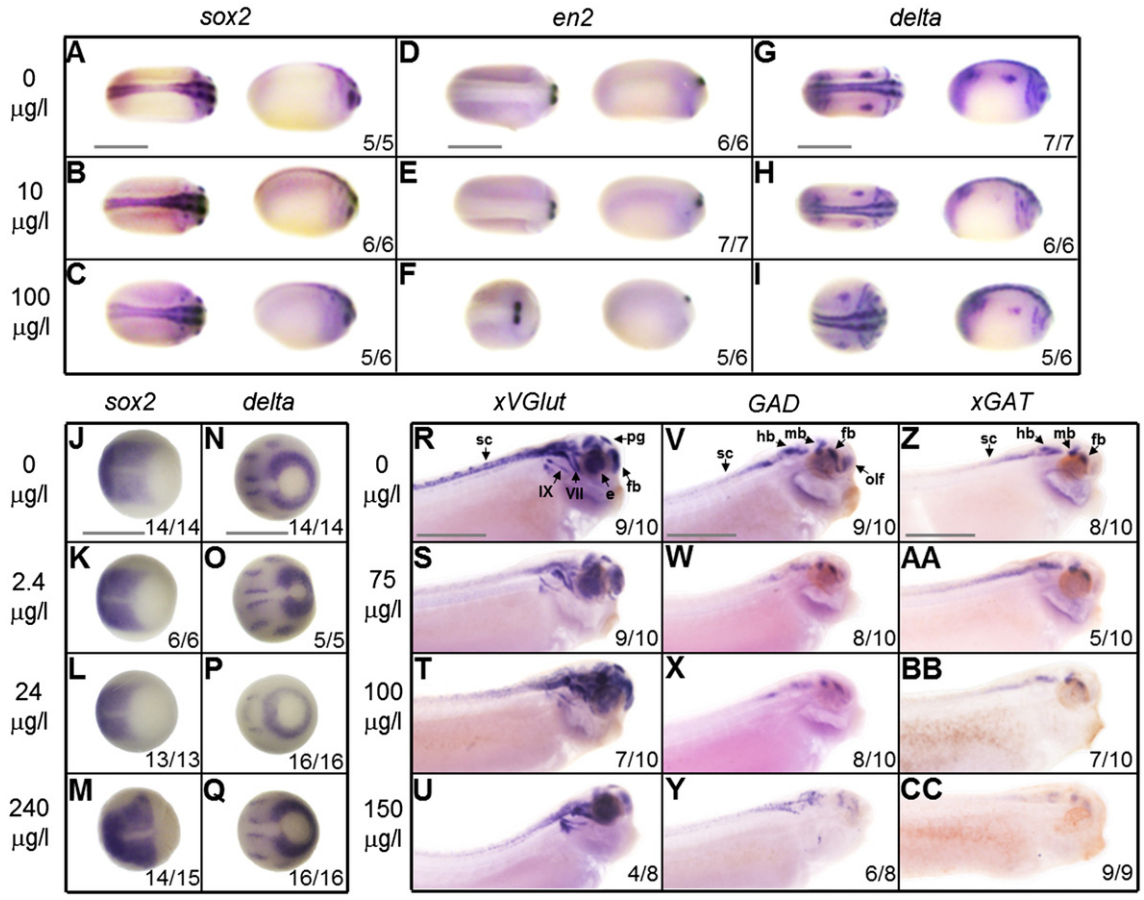

Fig. 4. Expression of early neural patterning and late neural phenotype genes in embryos exposed to varying concentrations of MeHgCl in solution, as assayed by ISH. Stages 23–24 embryos are seen from a dorsal (left) and lateral (right) view probed for *sox2* (A–C), *en2* (D–F), and *delta* (G–I). Similarly, shown is the dorsal view of stage 12 embryos probed *sox2* (J–M) and *delta* (N–Q). For neural phenotypes, a lateral view of stage 35 embryos is shown stained for *xVGlut* (R–U), *GAD* (V–Y) and *xGAT* (Z–CC) expression. Dark purple-blue areas indicate positive expression of mRNA. For all images, anterior is on the right, and for lateral views dorsal is up. N = 2 experiments, with the total number of evaluated embryos shown at the lower right of each image. The number of embryos out of the total matching each image is also shown; where counts were evenly split, the embryos most similar to controls are displayed. Abbreviations: e, eye; fb, forebrain; hb, hindbrain; mb, midbrain; olf, olfactory; pg, pineal gland; sc, spinal cord; VII, cranial nerve VII; VIII, cranial nerve VIII; IX, cranial nerve IX. Scale bars represent 1 mm.

was misexpression in neural regions (Fig. 4t) and cranial nerves (Fig. 4u) with increasing dose (Fig. 4r–u). For both *GAD* and x*GAT*, there was a noted decrease in the number of embryos with proper patterning with higher MeHgCl exposure, along with a decrease in observable signal strength, particularly in the midbrain and forebrain regions (Fig. 4v–cc). These effects were most apparent in embryos with greater overall deformity.

3.3. PCNA and TUNEL display a decrease of cell proliferation and increase of death in response to MeHg

As morphological disruption began during neurulation for all treatments, despite normal expression of neural patterning genes, embryos were examined for *PCNA* transcription as a marker of proliferation to investigate if MeHg was preventing proper production of neural cells during neurulation. Alterations in *PCNA* patterning and intensity were observed by ISH, and became more pronounced with treatment dose (Fig. 5). Expression of *PCNA* was first visible around stage 13 during the first wave of neurogenesis (Hartenstein, 1989), and a qualitative reduction in *PCNA* signal and area of expression was seen in the posterior neural folds of the embryonic neural plate during neural fold stages 14–15 at the highest two MeHg concentrations (150–200 µg/l) (Fig. 5e,f). Disruption of *PCNA* based on dose and stage occurred when developmental abnormalities became apparent (Table 1). qRT-PCR quantitation of *PCNA* expression, found a decrease in the relative amount of *PCNA* transcripts at 75 and 150 µg/l MeHgCl compared to the 0 µg/l control, with ΔΔCT scores that were 1.72 ± 0.26 and 1.62 ± 0.42 cycles above the control, respectively; corresponding to a 60% and 57% respective reduction in *PCNA* transcripts after $2^{-\Delta\Delta C_T}$ transformation (N = 1 experiment, 3 technical replicates, 10 embryos total for each dose) (Fig. 5y). Histological sections of stages 37–38 embryos exposed to 100 µg/l MeHgCl displayed a similar trend. Embryos that grew normally showed greater, but still less than that of control, *PCNA* expression in neural regions, while embryos with gross morphological disruption had a greatly reduced level of expression and a reduced neural region — particularly in the forebrain areas (Fig. 6). Quantitation of cell number was performed on the histological sections using DAPI staining of nuclei and cell counting with ImageJ. A statistically significant reduction in the number of neural cells was observed in the forebrain (N = 4 experiments, 7 embryos at 0 µg/l and 8 at 100 µg/l total; $p = 0.039$) and spinal cord ($p = 0.0056$) regions of stage 37 embryos exposed to 100 µg/l MeHg compared to controls (Fig. 6i). While not statistically significant in the midbrain or hindbrain regions ($p = 0.25$ and $p = 0.30$, respectively), these results support a reduction in neural cell proliferation as a contributing mechanism to the decrease in *GAD* and *xGAT* expression and general neural developmental disruption.

A marked increase in apoptosis measured by TUNEL positive cells was observed in embryos exposed to 100 µg/l MeHgCl, compared to siblings grown in standard rearing conditions (Fig. 7). The increase in TUNEL positive cells appeared to be stage dependent, embryos before stages 14–15 did not demonstrate as large a rise in positives relative to controls, compared to embryos at stages 19–20 and older. Histological analysis showed the increase in TUNEL labeled cells to be mostly in the neural and epidermal regions of the embryo, and appeared to

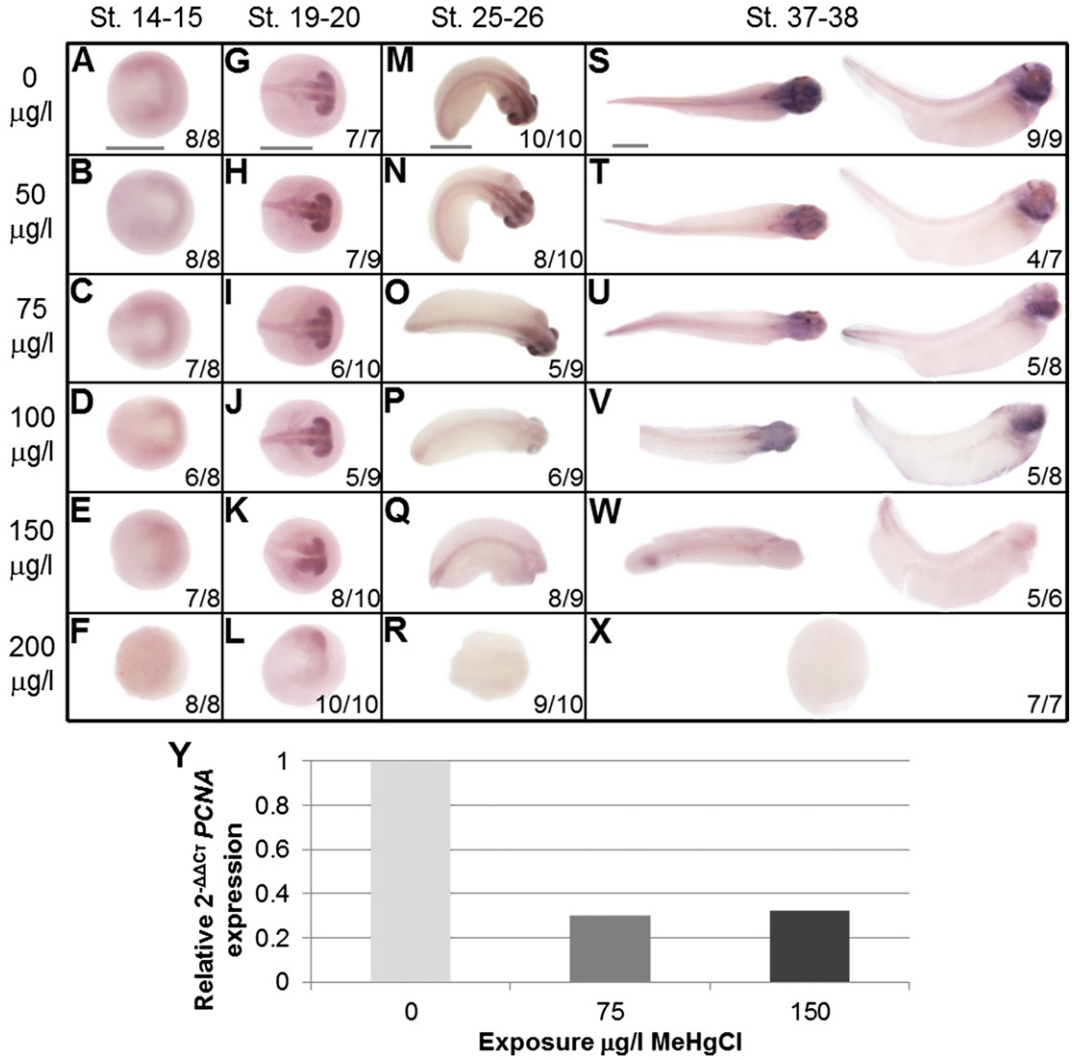

Fig. 5. Expression pattern of *PCNA* at several developmental stages during MeHgCl solution exposure, as detected by ISH. Stages 14–15 (A–F), stages 19–20 (G–L), and stages 25–26 (M–R) embryos are seen from a dorsal view. Stages 37–38 embryos (S–X) are shown from a dorsal (left) and lateral (right) view, except for 200 µg/l, which is a featureless ball of cells. All embryos shown are representative near the average phenotype score from exposure at each dose. For all images, anterior is on the right. Dark purple-blue areas indicate positive *PCNA* expression. N = 2 experiments, with the total number of evaluated embryos shown at the lower right of each image. The number of embryos out of the total matching each image is also shown. (Y) qRT-PCR results of relative *PCNA* expression in stage 37 embryos at each MeHgCl dose. Values for the ΔΔCT score in each condition have been normalized to the expression level of the 0 µg/l control and are shown using $2^{-\Delta\Delta C_T}$ scale. N = 1 biological experiment pooled from 10 embryos, and 3 technical replicates, for each dose. Scale bars represent 1 mm.

have the highest localization in the cell dense periventricular zones (Fig. 8). Counts of TUNEL positive cells in stage 37 embryos from histological sections displayed a statistically significant increase in the number of apoptotic cells per 100 neural nuclei in the forebrain (N = 2 experiments, and 3 sectioned embryos per dose; $p = 10^{-6}$) and spinal cord ($p = 0.019$) compared to unexposed controls (Fig. 8i). Both the midbrain and hindbrain showed a decreased number of nuclei and an increase in apoptotic cells compared to controls, but were not statistically significant ($p = 0.25$ and $p = 0.099$ for midbrain, respectively; $p = 0.30$ and $p = 0.11$ for hindbrain, respectively). To try to investigate the pathways involved in apoptosis, embryos were injected with 4.6 nl of 1 mM (for a final 10 µM concentration) of Pifithrin-µ to inhibit p53 activated apoptosis (Storm et al., 2006), or MDL28170 to inhibit the Bax activation step by calpains (Briz et al., 2013) prior to exposure to 0 or 100 µg/l MeHgCl (N = 3 experiments, 20 embryos total for each dose and inhibitor). While a 40–50% rescue was seen of embryos exposed to positive controls of H_2O_2 and ethanol for each pathway, respectively, no impact on 100 µg/l MeHgCl induced phenotypes was observed, and nor was a change seen in Bax or p53 expression by ISH in response to MeHgCl exposure (data not shown).

3.4. Microarray analysis shows cell cycle and apoptosis pathways are affected, but not neural patterning genes

To analyze global gene transcription changes during the start of neural progenitor, regional patterning gene expression, and MeHg induced developmental disruption, whole transcriptome microarray analysis was carried out on late gastrulation stage 12 embryos exposed to 200 µg/l of MeHgCl at 2 e/ml. Of the 32,475 genes in the Affymetrix array, 7453 genes were found to be significantly differentially expressed ($p < 0.05$) (Supplementary Table 1). No significant changes were found for *sox2*, *en2*, or *delta*, as verified by ISH (Table 2), or the *notch* receptor ($p = 0.15$). *PCNA* was significantly upregulated at this stage in response to MeHg exposure (Table 2; $p = 0.0064$), although it could not be distinguished from background staining by ISH. As *PCNA* did not show a loss of patterning until later stages at this dose, this difference is consistent with early or compensatory transcriptional changes prior to disruption of cell proliferation.

In order to analyze which gene pathways were being affected, pathway enrichment analysis of differentially expressed genes using Partek was performed. Eight pathways were found as significantly enriched

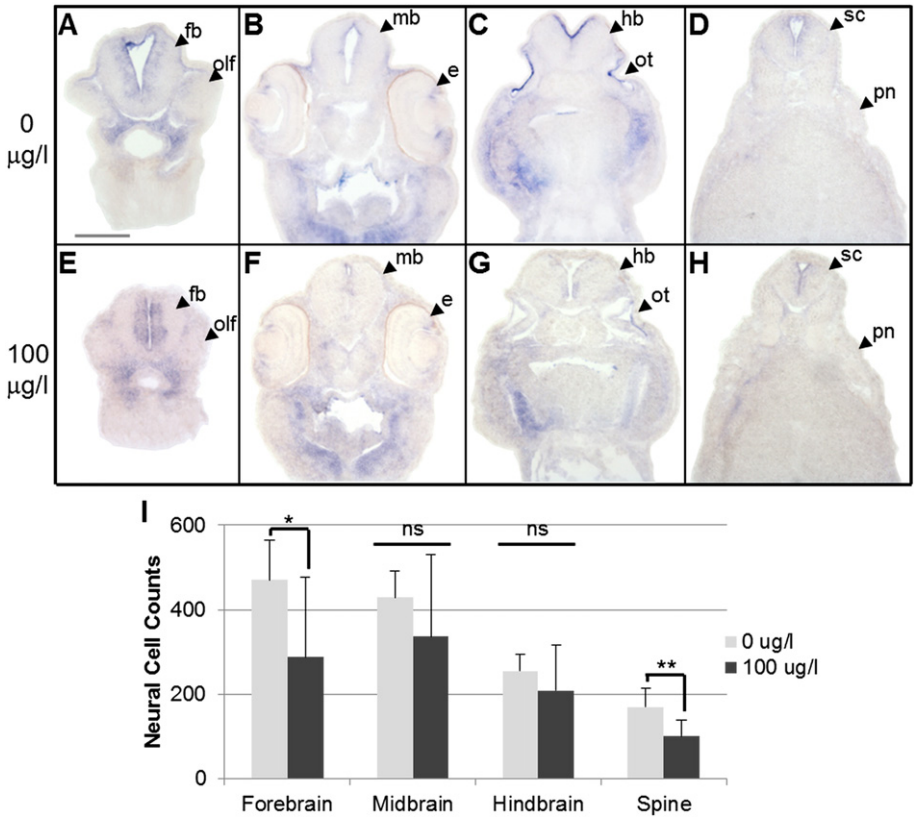

Fig. 6. Transverse histological cryosections through stage 37 embryos stained for *PCNA* expression (blue regions) by ISH. Forebrain, midbrain, hindbrain, and spinal cord sections of control (A–D) and MeHgCl solution exposed (E–H) embryos are shown oriented dorsal on top. Two of the four MeHgCl exposed embryos displayed abnormally reduced or absent forebrain structures as seen in (E). N = 2 experiments, with 4 embryos sectioned from each condition. (I) Neural cell counts using DAPI stain compared between unexposed and MeHgCl exposed embryos averaged over each CNS region. N = 4 experiments, with 7 embryos sectioned from 0 µg/l and 8 from 100 µg/l total. Error bars represent standard deviation. *p = 0.039, **p = 0.0056, ns = not significant as determined by Student's *t*-test for each region. Abbreviations: e, eye; fb, forebrain; hb, hindbrain; mb, midbrain; olf, olfactory; ot, otic vesicle; pn, pronephros; sc, spinal cord. Scale bar represents 150 µm.

($p < 0.05$), including cell cycle ($p = 0.0003$) and apoptosis ($p = 0.049$) pathways. Developmental processes were not significantly altered according to this analysis, but were significantly altered ($p < 0.05$) according to GO term enrichment (Supplementary Table 2), suggesting that other development related genes may be affected by MeHg exposure.

4. Discussion

MeHgCl exposure was found to be a potent teratogen to the developing nervous system of *X. laevis* embryos within a range of concentrations below and up to the lower limit in adult human blood (200 µg/l) where

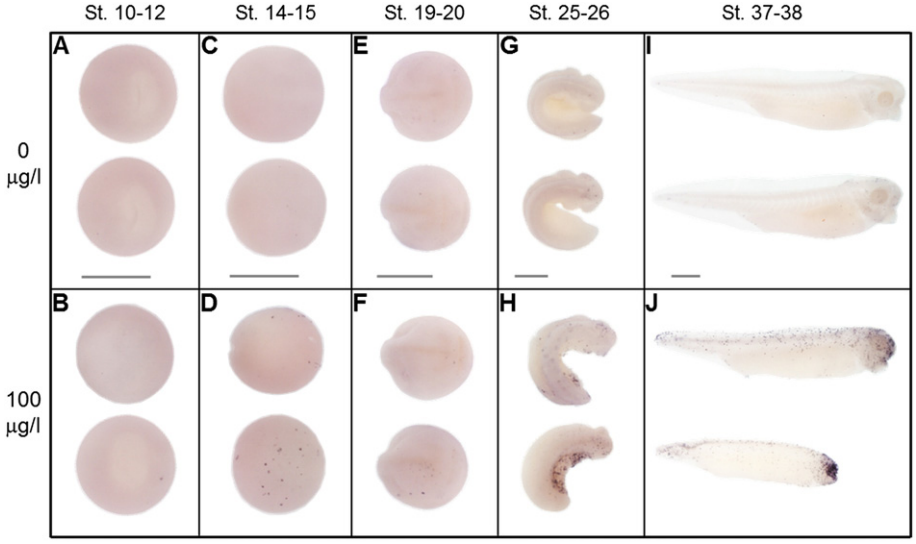

Fig. 7. TUNEL staining for cells undergoing apoptosis in whole mount embryos exposed to MeHgCl solution. Shown dorsally are stages 10–12 (A–B), stages 14–15 (C–D), stages 19–20 (E–F), and stages 25–26 embryos (G–H). Stages 37–38 embryos (I–J) are seen from a lateral view. For all images, anterior is on the right. For controls, a low (top) and high (bottom) staining embryo is shown. For the MeHgCl exposed, an average (top) and below average (bottom) ranked embryo is shown for each stage. N = 2 experiments, and 10 embryos total for each. Scale bars represent 1 mm.

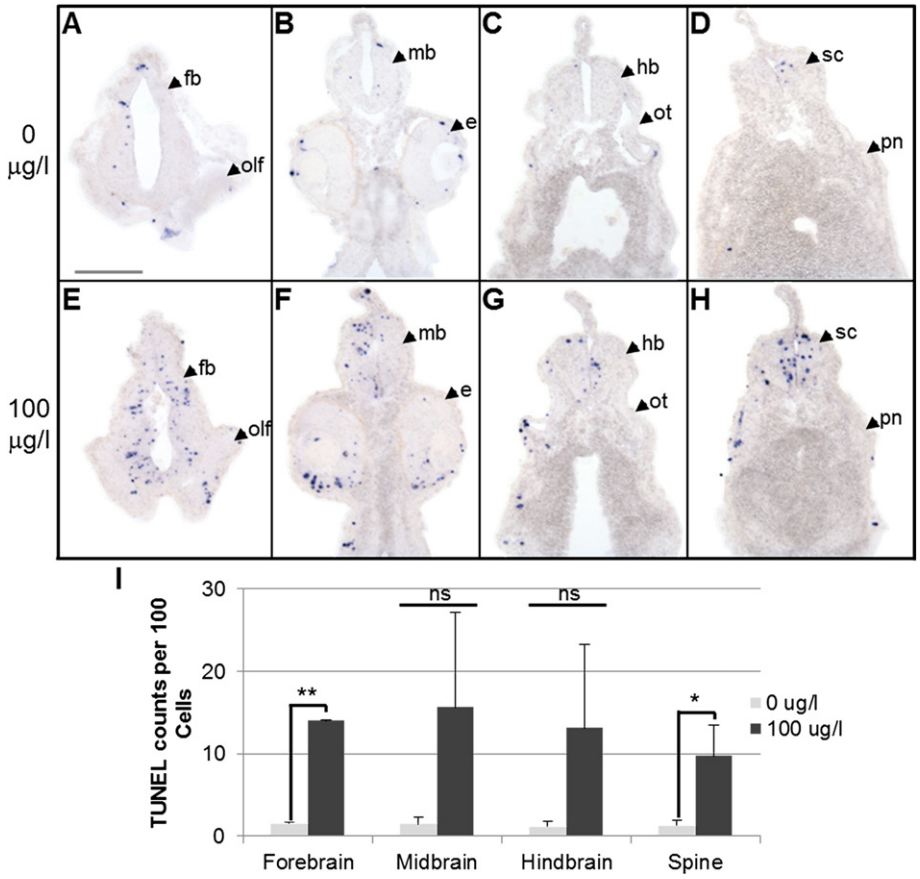

Fig. 8. Histological sections cut transversely by cryosectioning though stage 37 embryos stained for apoptotic cells (blue dots) by TUNEL assay. Forebrain, midbrain, hindbrain, and spinal cord sections of control (A–D) and MeHgCl solution exposed (E–H) embryos are shown oriented dorsal on top. N = 2 experiments, with 4 embryos sectioned from each concentration. (I) Number of TUNEL positive cells per 100 neural cells compared between unexposed and MeHgCl exposed embryos averaged over each CNS region. N = 2 experiments, with 3 embryos sectioned from each condition. Error bars represent standard deviation. *p = 0.019, **p = 10^{-6}, ns = not significant as determined by Student's *t*-test for each region. Abbreviations: e, eye; fb, forebrain; hb, hindbrain; mb, midbrain; olf, olfactory; ot, otic vesicle; pn, pronephros; sc, spinal cord. Scale bar represents 150 µm.

the first signs of toxicity (paresthesia) occur (USFDA, 1994). Dose response phenotype experiments gave a TC_{50} and LC_{50} for stage 37 embryos at 1 e/ml of ~50 µg/l and ~100 µg/l, respectively (Fig. 2a). This agrees with the TC_{50} and LC_{50} (~50 µg/l and ~70 µg/l) calculated from previous work in *X. laevis* exposed at unknown density for 120 h (approximately stage 47) (Prati et al., 2002), and the LC_{50} (~100–125 µg/l) observed in zebrafish at more similar developmental time points (Hassan et al., 2012; Ho et al., 2013 Supplementary Fig. 5). In addition to the concentration of MeHg in solution, we found that the density of the embryos played a statistically significant role ($p = 1.16 * 10^{-5}$ between 1 and 2 e/ml; $p = 4.19 * 10^{-12}$ between 2 and 3 e/ml) in the severity of the phenotypes displayed at a given dose, and on the consequent TC_{50} and LC_{50} (Fig. 2b,c). To our knowledge, this is the first report of the density of MeHg solution exposed embryos having such a large effect on toxicity response.

Table 2
Microarray fold change and p-values of genes assayed by ISH.

Gene	Probe set ID	Fold DE	Adjusted p-value
sox2	Xl.188.1.S2_a_at	−1.05	0.666
sox2	Xl.188.1.S2_at	−1.08	0.512
sox2	Xl.188.1.S1_a_at	−1.06	0.666
en2	Xl.1174.1.S1_at	−1.03	0.815
delta	Xl.54916.1.A1_s_at	−1	0.977
delta	Xl.14759.1.S1_at	−1.08	0.34
PCNA	Xl.34965.1.S1_at	1.56	0.00636

Throughout development, there was a statistically significant uptake of MeHg compared to that of controls ($p = 0.0006$) in a developmental stage ($p = 2.85 * 10^{-48}$) and dose ($p = 1.03 * 10^{-58}$) dependent manner, with a significant interaction between the two factors ($p = 1.88 * 10^{-21}$) (Fig. 3b). The rate of MeHg uptake was dependent on dose. By stage 4, only the highest dose had significant uptake (200 µg/l MeHgCl; $p = 0.00044$), but this included the lowest dose by stage 10 (50 µg/l; $p = 0.0066$). Consequently, the first signs of developmental abnormality in any experiment were observed at gastrula stages 10–12 in the highest three MeHgCl doses, while lower concentrations did not induce disruption until the neurula stages 18–20 (Table 1). The majority of abnormalities at all doses began during neurogenesis from stages 13–20 (Hartenstein, 1989) despite different rates of MeHg uptake, demonstrating a greater vulnerability of embryos at neurula stage than gastrula (Falluel-Morel et al., 2007; Rand et al., 2009; Guo et al., 2013). At the three lowest doses, the concentration of mercury in embryos plateaued to comparable levels by stage 37, and the highest dose (200 µg/l) reached only 1.7 times the mercury in tissue than the lowest (50 µg/l) by stage 45 (Fig. 3b). This suggests that a steady state or buffering system is involved in embryonic MeHg tissue loads, which is overwhelmed at high levels of exposure as seen in tadpoles fed contaminated food during metamorphosis (Davidson et al., 2011). Despite this, increasing MeHg exposure resulted in greater embryonic disruption and lethality (Fig. 3a), indicating that transient flux or higher early levels of uptake, particularly during neurulation, may play a larger role in developmental toxicity than the endpoint concentration measured at tadpole stage.

Early neural progenitor and patterning gene markers *sox2*, *en2*, and *delta* were found to show no evidence of change, even at the highest MeHg doses in this study (Fig. 4). Microarray analysis at stage 12 (before the stages used for phenotyping), the start of neural progenitor and differentiation gene expression (Ferreiro et al., 1994; Kishi et al., 2000), found no significant differential expression of those genes from MeHgCl exposure (Table 2), despite observable abnormalities by that stage at that dose (200 μg/l) (Table 1). This agrees with *sox2* expression in zebrafish at older stages (48 to 72 hpf), which showed no significant change at a lower concentration of MeHg (60 μg/l) (Ho et al., 2013). Thus, failures in neural development and subsequent neurological problems are not likely explained by losses of early nervous system patterning by these genes. Investigation of the inhibitory neuronal phenotype markers *GAD* and *xGAT* found a qualitative decrease in expression strength and the number of embryos with normal patterning (Fig. 4v–cc), while excitatory neurons labeled by *xVGlut* did not show as much a decrease, but began to have areas of misexpression (Fig. 4r–u). This implies other mechanisms besides early neural patterning could be leading to a lack of neuronal differentiation or the loss of subpopulations of neurons, and in particular those with an inhibitory phenotype as suggested in rats (O'Kusky et al., 1988; Yuan and Atchison, 1997) and minks (Basu et al., 2010).

Unlike early neural patterning genes, expression of *PCNA* was found to correlate with embryological phenotype, with greater levels of deformity showing reduced areas of *PCNA* expression (Figs. 5 and 6). Levels of *PCNA* were highest in presumptive neural regions of control embryos starting at stage 13, and the reduction of *PCNA* expression upon MeHgCl exposure appeared to affect those regions most severely, as observed with embryos that lacked anterior brain regions yet otherwise appeared normal (Figs. 3c; 5k,q). Cell counts of transverse histological sections revealed a statistically significant decrease in the number of neural nuclei in the forebrain ($p = 0.039$) and spinal cord ($p = 0.0056$) (Fig. 6i), and qRT-PCR found a reduction of *PCNA* transcripts upwards of 60% (Fig. 5y). This agrees with the decreased PCNA protein levels in zebrafish neural tissue exposed to MeHg (50 μg/l and 80 μg/l) (Hassan et al., 2012) at a comparable density (1 to 1.5 e/ml). Microarray studies of zebrafish, however, did not appear to find differential expression of cell cycle genes or *PCNA* (Yang et al., 2007; Ho et al., 2013), although one of those studies noted reduced brain size in MeHg treated embryos (Ho et al., 2013). A possible explanation for this difference may be the higher embryo density (5 e/ml) reported by Ho et al. (2013), supporting the observation that embryonic density impacts developmental response to MeHg and could confound between-study comparisons. In our microarray at stage 12, *PCNA* expression showed significant upregulation (1.54 folds, $p = 0.00636$) (Table 2). However, ISH staining at stage 12 and earlier could not distinguish *PCNA* expression from background, suggesting that a loss of *PCNA* expression occurs after the developmental point used on the microarray. Early upregulation by stage 12 may be related to *PCNA*'s role in DNA repair rather than cell proliferation (Prevodnik et al., 2007; Chen et al., 2013), and may represent an early stress response to MeHg.

The number of apoptotic cells detected by TUNEL was significantly increased from MeHg exposure (Figs. 7 and 8), particularly of neural cells in the forebrain ($p = 1 * 10^{-6}$) and spinal cord ($p = 0.019$) (Fig. 8i), coinciding with the decreased cell counts (Fig. 6i). While the pattern of cell death did not appear to have structurally specific localizations, apoptosis was highest in neural regions near the ventricle (Fig. 8e–h). The combination of lowered cell proliferation and increased cell death in neural tissue provides a possible mechanism for the sensitivity of the neurula stages to MeHg, through the disruption of neurogenesis and neural survival during this critical point. Likewise, microarray analysis of adult zebrafish brain tissue after intraperitoneal injection of MeHg found significant alteration of gene pathways regulating cell survival and apoptosis in favor of cell death (Richter et al., 2011). And a decreased neural proliferation and increased cell death in the hippocampus of rats exposed perinatally to MeHg lead to impairment in memory function lasting through adolescence (Falluel-Morel et al., 2007; Sokolowski et al., 2013). In our stage 12 embryos, microarray results displayed a strong upregulation of mitochondrial associated apoptotic genes such as cytochrome c ($p < 0.005$) and caspase 9 ($p < 0.03$), but found a downregulation of bax ($p < 0.012$) and no significant change in caspase 8 ($p > 0.08$), caspase 3 ($p > 0.07$), or p53 ($p > 0.5$). Injection of the apoptosis inhibitors Pifithrin-μ or MDL28170 found no rescue of phenotypes or embryonic lethality, suggesting MeHg induced apoptosis does not solely involve p53 or calpain induction of Bax, respectively.

In conclusion, MeHg toxicity disrupted *X. laevis* embryogenesis most severely during development of the nervous system from stages 13 to 20, coinciding with both the first and second waves of neurogenesis (Hartenstein, 1989). While early neural patterning and progenitor gene expression remained largely unaffected, later neuronal phenotype expression of GABAergic populations was reduced. This was also reflected in a loss of cell proliferation in areas of nervous system development, and an increase in apoptosis. This suggests the loss of neural populations is through a mechanism of decreased proliferation and increased cell death early in neurulation, rather than neural patterning gene disruption, as supported by studies in mice and rats at later developmental points (Sakamoto et al., 2004; Glover et al., 2009; Radonjic et al., 2013). Further work remains to be done to determine additional mechanisms, especially those underlying the occurrence of failed neural tube closure seen in neurula stages at higher doses (Fig. 5k,q). Investigation of the role of calcium during these events could provide additional insight due to observed antagonism of calcium channels by MeHg (Yuan et al., 2005), and the importance of calcium in cell migration and neural phenotype specification. Recently, frequent calcium spiking in neural progenitors, suggested to be inhibited by MeHg (Fahrion et al. 2012; Kong et al. 2013), has been implicated to lead to a GABAergic phenotype (Marek et al., 2010; Lewis et al., 2014), providing an additional possible mechanism for the enhanced downregulation of inhibitory neuronal populations by MeHg and the resulting neurological sensory and motor defects.

Supplementary data to this article can be found online at http://dx.doi.org/10.1016/j.ntt.2014.11.010.

Transparency document

The Transparency document associated with this article can be found in the online version.

Conflict of interest

Nothing declared.

Acknowledgments

Funding for this work came from NIH grants R15HD077624-01 and 1R15HD077624-01 to MSS, NSF grant IOS-1527895 to MSS, Charles Center grant 2010-2011 to MN and NO, and the Howard Hughes Medical Institute Undergraduate Science Education program grant to the College of William and Mary provided to MN and NO. We thank Lidia Epp for providing DNA sequencing service, and Vollter Anastas, Catherine Bianchi, Andrew Halleran, Morgan Sehdev, and Monika E. Stanciauskas for assistance in manuscript proof reading; as well as our reviewers for their insightful comments. We also thank Dan Cristol for support in using the DMA-80.

References

Amyot M, Morel FMM, Ariya PA. Dark oxidation of dissolved and liquid elemental mercury in aquatic environments. Environ Sci Technol 2005;39:110–4. http://dx.doi.org/10.1021/es035444k.

Basu N, Scheuhammer AM, Rouvinen-Watt K, Evans RD, Trudeau VL, Chan LH. *In vitro* and whole animal evidence that methylmercury disrupts GABAergic systems in discrete brain regions in captive mink. Comp Biochem Physiol C Toxicol Pharmacol 2010; 151(3):379–85. http://dx.doi.org/10.1016/j.cbpc.2010.01.001.

Benjamini Y, Hochberg Y. Controlling the false discovery rate: a practical and powerful approach to multiple testing. J R Stat Soc B 1995;57(1):289–300. http://dx.doi.org/10.2307/2346101.

Bertossi M, Girolamo F, Errede M, Virgintino D, Elia G, Ambrosi L, et al. Effects of methylmercury on the microvasculature of the developing brain. Neurotoxicology 2004;25:849–57. http://dx.doi.org/10.1016/j.neuro.2004.01.005.

Bisen-Hersh EB, Farina M, Barbosa Jr F, Rocha JB, Aschner M. Behavioral effects of developmental methylmercury drinking water exposure in rodents. J Trace Elem Med Biol 2014;28(2):117–24. http://dx.doi.org/10.1016/j.jtemb.2013.09.008.

Briz V, Hsu YT, Li Y, Lee E, Bi X, Baudry M. Calpain-2-mediated PTEN degradation contributes to BDNF-induced stimulation of dendritic protein synthesis. J Neurosci 2013;33(10):4317–28. http://dx.doi.org/10.1523/JNEUROSCI.4907-12.2013.

Byun J, Verardo MR, Sumengen B, Lewis GP, Manjunath BS, Fisher SK. Automated tool for the detection of cell nuclei in digital microscopic images: application to retinal images. Mol Vis 2006;12:949–60.

Carvalhol CM, Chew EH, Hashemy SI, Lu J, Holmgren A. Inhibition of the human thioredoxin system. A molecular mechanism of mercury toxicity, J Biol Chem 2008;283(18):11913–23. http://dx.doi.org/10.1074/jbc.M710133200.

Chen X, Paudyal SC, Chin RI, You Z. PCNA promotes processive DNA end resection by Exo1. Nucleic Acids Res 2013;41(20):9325–38. http://dx.doi.org/10.1093/nar/gkt672.

Chumchal MM, Rainwater TR, Osborn SC, Roberts AP, Abel MT, Cobb GP, et al. Mercury speciation and biomagnification in the food web of Caddo Lack, Texas and Louisiana, USA, a subtropical freshwater ecosystem. Environ Toxicol Chem 2011;30(5):1153–62. http://dx.doi.org/10.1002/etc.477.

Davidson MA, Croteau MC, Millar CS, Trudeau VL, Lean DR. Fate and developmental effects of dietary uptake of methylmercury in *Silurana tropicalis* tadpoles. J Toxicol Environ Health A 2011;74(6):364–79. http://dx.doi.org/10.1080/15287394.2011.534427.

Engel GL, Delwig A, Rand MD. The effects of methylmercury on Notch signaling during embryonic neural development in *Drosophila melanogaster*. Toxicol *In Vitro* 2012;26:485–92. http://dx.doi.org/10.1016/j.tiv.2011.12.014.

Engel GL, Rand MD. The Notch target E (spl) mδ is a muscle-specific gene involved in methylmercury toxicity in motor neuron development. Neurotoxicol Teratol 2014;43:11–8. http://dx.doi.org/10.1016/j.ntt.2014.03.001.

Fahrion JK, Komuro Y, Li Y, Ohno N, Littner Y, Raoult E, Galas L, Vaudry D, Komuro H. Rescue of neuronal migration deficits in a mouse model of fetal Minamata disease by increasing neuronal Ca^{2+}spike frequency. Proc Natl Acad Sci USA 2012;109(13):5057–62. http://dx.doi.org/10.1073/pnas.1120747109.

Falluel-Morel A, Sokolowski K, Sisti HM, Zhou X, Shors TJ, DiCicco-Bloom E. Developmental mercury exposure elicits acute hippocampal cell death, reductions in neurogenesis, and severe learning deficits during puberty. J Neurochem 2007;103(5):1968–81. http://dx.doi.org/10.1111/j.1471-4159.2007.04882.x.

Ferreiro B, Kintner C, Zimmerman K, Anderson D, Harris WA. XASH genes promote neurogenesis in *Xenopus* embryos. Development 1994;120:3649–55.

Gentleman RC, Carey VJ, Bates DM, Bolstad B, Dettling M, Dudoit S, et al. Bioconductor: open software development for computational biology and bioinformatics. Genome Biol 2004;5(10):R80. http://dx.doi.org/10.1186/gb-2004-5-10-r80.

Gleason KK, Dondeti VR, Hsia HL, Cochran ER, Gumulak-Smith J, Saha MS. The vesicular glutamate transporter 1 (xVGlut1) is expressed in discrete regions of the developing *Xenopus laevis* nervous system. Gene Expr Patterns 2003;3(4):503–7. http://dx.doi.org/10.1016/S1567-133X(03)00057-7.

Glover CN, Zheng D, Jayahankar S, Sales GD, Hogstrand C, Lundebye AK. Methylmercury speciation influences brain gene expression and behavior in gestationally-exposed mice pups. Toxicol Sci 2009;110:389–400. http://dx.doi.org/10.1093/toxsci/kfp105.

Guo BQ, Yan CH, Cai SZ, Yuan XB, Shen XM. Low level prenatal exposure to methylmercury disrupts neuronal migration in the developing rat cerebral cortex. Toxicology 2013;304:57–68. http://dx.doi.org/10.1016/j.tox.2012.11.019.

Harland RM. *In situ* hybridization: an improved whole-mount method for *Xenopus* embryos. Methods Cell Biol 1991;36:685–95.

Harris RC, Rudd JWM, Amyot M, Babiarz CL, Beaty KG, Blanchfield PJ, et al. Whole-ecosystem study shows rapid fish–mercury response to changes in mercury deposition. PNAS 2007;104(42):16586–91. http://dx.doi.org/10.1073/pnas.0704186104.

Hartenstein V. Early neurogenesis in *Xenopus*: the spatio-temporal pattern of proliferation and cell lineages in the embryonic spinal cord. Neuron 1989;3(4):399–411. http://dx.doi.org/10.1016/0896-6273(89)90200-6.

Hassan SA, Moussa EA, Abbot LC. The effect of methylmercury exposure on early central nervous system development in the zebrafish (*Danio rerio*) embryo. J Appl Toxicol 2012;32:707–13. http://dx.doi.org/10.1002/jat.1675.

Hemmati-Brivanlou A, de la Torre JR, Holt C, Harland RM. Cephalic expression and molecular characterization of *Xenopus* En-2. Development 1991;111(3):715–24.

Ho NY, Yang L, Legradi J, Armant O, Takamiya M, Rastegar S, et al. Gene responses in the central nervous system of zebrafish embryos exposed to the neurotoxicant methyl mercury. Environ Sci Technol 2013;47:3316–25. http://dx.doi.org/10.1021/es3050967.

Horvat M, Degenek N, Lipei L, Snoj Tratnik J, Faganeli J. Trophic transfer and accumulation of mercury in ray species in coastal waters affected by historic mercury mining (Gulf of Trieste, northern Adriatic Sea). Environ Sci Pollut Res Int 2013;21(6):4163–76. http://dx.doi.org/10.1007/s11356-013-2262-0.

Irizarry RA, Hobbs B, Collin F, Beazer-Barclay YD, Antonellis KJ, Scherf U, et al. Exploration, normalization, and summaries of high density oligonucleotide array probe level data. Biostatistics 2003;4(2):249–64. http://dx.doi.org/10.1093/biostatistics/4.2.249.

Kishi M, Mizuseki K, Sasai N, Yamazaki H, Shiota K, Nakanishi S, et al. Requirement of *Sox2*-mediated signaling for differentiation of early *Xenopus* neuroectoderm. Development 2000;127:791–800.

Kong HK, Wong MH, Chan HM, Lo SC. Chronic exposure of adult rats to low doses of methylmercury induced a state of metabolic deficit in the somatosensory cortex. J Proteome Res 2013;12(11):5233–45. http://dx.doi.org/10.1021/pr400356v.

Lewis BB, Miller LE, Herbst WA, Saha MS. The role of voltage-gated calcium channels in neurotransmitter phenotype specification: coexpression and functional analysis in *Xenopus laevis*. J Comp Neurol 2014;522(11):2518–31. http://dx.doi.org/10.1002/cne.23547.

Li M, Sipe CW, Hoke K, August LL, Wright MA, Saha MS. The role of early lineage in GABAergic and glutamatergic cell fate determination in *Xenopus laevis*. J Comp Neurol 2006;495(6):645–57. http://dx.doi.org/10.1002/cne.20900.

Marek KW, Kurtz LM, Spitzer NC. cJun integrates calcium activity and tlx3 expression to regulate neurotransmitter specification. Nat Neurosci 2010;13(8):944–50. http://dx.doi.org/10.1038/nn.2582.

Mergler D, Anderson HA, Chan LH, Mahaffey KR, Murray M, Sakamoto M, et al. Methylmercury exposure and health effects in humans: a worldwide concern. Ambio 2007;36(1):3–11. http://dx.doi.org/10.1579/0044-7447(2007)36[3:MEAHEI]2.0.CO;2.

Monetti C, Vigetti D, Prati M, Sabbioni E, Bernardini G, Gornati R. Gene expression in *Xenopus* embryos after methylmercury exposure: a search for molecular biomarkers. Environ Toxicol Chem 2002;21(12):2731–6. http://dx.doi.org/10.1897/1551-5028(2002)021<2731:GEIXEA>2.0.CO;2.

Nieuwkoop PD, Faber J. Normal table of *Xenopus laevis* (Daudin). New York: Garland Publishing Inc.; 1994.

O'Kusky JR, Radke JM, Vincent SR. Methylmercury-induced movement and postural disorders in developing rat: loss of somatostatin-immunoreactive interneurons in the striatum. Brain Res 1988;468(1):11–23.

Padhi BK, Pelletier G, Williams A, Berndt-Weis L, Yauk C, Bowers WJ, et al. Gene expression profiling in rat cerebellum following in utero and lactational exposure to mixtures of methylmercury, polychlorinated biphenyls and organochlorine pesticides. Toxicol Lett 2008;176(2):93–103. http://dx.doi.org/10.1016/j.toxlet.2007.08.016.

Patel E, Reynolds M. Methylmercury impairs motor function in early development and induces oxidative stress in cerebellar granule cells. Toxicol Lett 2013;222(3):265–72. http://dx.doi.org/10.1016/j.toxlet.2013.08.002.

Prati M, Gornati R, Boracchi P, Biganzoli E, Fortaner S, Pietra R, et al. A comparative study of the toxicity of mercury dichloride and methylmercury assayed by the Frog Embryo Teratogenesis Assay—*Xenopus* (FETAX). Altern Lab Anim 2002;30(1):23–32.

Prevodnik A, Lilja K, Bollner T. Benzo [*a*] pyrene up-regulates the expression of the proliferating cell nuclear antigen (PCNA) and multixenobiotic resistance polyglycoprotein (P-gp) in Baltic Sea blue mussels (*Mytilus edulis* L.). Comp Biochem Physiol C Toxicol Parmacol 2007;145:265–74. http://dx.doi.org/10.1016/j.cbpc.2006.12.014.

Radonjic M, Cappaert NL, de Vries EF, de Esch CE, Kuper FC, van Waarde A, et al. Delay and impairment in brain development and function in rat offspring after maternal exposure to methylmercury. Toxicol Sci 2013;133(1):112–24. http://dx.doi.org/10.1093/toxsci/kft024.

Rand MD, Bland CE, Bond J. Methylmercury activates enhancer-of-split and bearded complex genes independent of the notch receptor. Toxicol Sci 2008;104(1):163–76. http://dx.doi.org/10.1093/toxsci/kfn060.

Rand MD, Dao JC, Clason TA. Methylmercury disruption of embryonic neural development in *Drosophila*. Neurotoxicology 2009;30(5):794–802. http://dx.doi.org/10.1016/j.neuro.2009.04.006.

Richter CA, Garcia-Reyero N, Martyniuk C, Knoebl I, Marie P, Wright-Osment MK, et al. Gene expression changes in female zebrafish (*Danio rerio*) brain in response to acute exposure to methylmercury. Environ Toxicol Chem 2011;30(2):301–8. http://dx.doi.org/10.1002/etc.409.

Sakamoto M, Kakita A, de Oliveira RB, Sheng Pan H, Takahashi H. Dose-dependent effects of methylmercury administered during neonatal brain spurt in rats. Brain Res Dev Brain Res 2004;152(2):171–6. http://dx.doi.org/10.1016/j.devbrainres.2004.06.016.

Schaefer JK, Rocks SS, Zheng W, Liang L, Baohua G, Morel FMM. Active transport, substrate specificity, and methylation of Hg (II) in anaerobic bacteria. PNAS 2011;108(21):8714–9. http://dx.doi.org/10.1073/pnas.1105781108.

Schmitt CJ, Striker CA, Brumbaugh WG. Mercury bioaccumulation and biomagnification in Ozark stream ecosystems. Ecotoxicol Environ Saf 2011;74(8):2215–24. http://dx.doi.org/10.1016/j.ecoenv.2011.08.008.

Simmons-Willis TA, Koh AS, Clarkson TW, Ballatori N. Transport of a neurotoxicant by molecular mimicry: the methylmercury-L-cysteine complex is a substrate for human L-type large neutral amino acid transporter (LAT) 1 and LAT2. Biochem J 2002;367(1):239–46. http://dx.doi.org/10.1042/BJ20020841.

Smyth GK. Linear models and empirical Bayes methods for assessing differential expression in microarray experiments. Stat Appl Genet Mol Biol 2005;3. http://dx.doi.org/10.2202/1544-6115.1027. [Article 3a].

Spada L, Annicchiarico C, Cardellicchio N, Giandomenico S, Di Leo A. Mercury and methylmercury concentrations in Mediterranean seafood and surface sediments, intake evaluation and risk for consumers. Int J Hyg Environ Health 2012;215(3):418–26. http://dx.doi.org/10.1016/j.ijheh.2011.09.003.

Sokolowski K, Obiorah M, Robinson K, McCandlish E, Buckley B, DiCicco-Bloom E. Neural stem cell apoptosis after low-methylmercury exposures in postnatal hippocampus produce persistent cell loss and adolescent memory deficits. Dev Neurobiol 2013;73(12):936–49. http://dx.doi.org/10.1002/dneu.22119.

Storm E, Sathe S, Komarov PG, Chernova OB, Pavlovska I, Shyshynova I, et al. Small-molecule inhibitor of p53 binding to mitochondria protects mice from gamma radiation. Nat Chem Biol 2006;2(9):474–9. http://dx.doi.org/10.1038/nchembio809.

Stringari J, Nunes AKC, Franco JL, Bohrer D, Garcia SC, Dafre AL, et al. Prenatal methylmercury exposure hampers glutathione antioxidant system ontogenesis and causes long-lasting oxidative stress in the mouse brain. Toxicol Appl Pharmacol 2008;227(1):147–54. http://dx.doi.org/10.1016/j.taap.2007.10.010.

USFDA. Mercury in fish: cause for concern? FDA Consumer; 1994 [Revised 1995].

Varian-Ramos CW, Condon AM, Hallinger KK, Carlson-Drexler KA, Cristol DA. Stability of mercury concentrations in frozen avian blood samples. Bull Environ Contam Toxicol 2011;86(2):159–62. http://dx.doi.org/10.1007/s00128-010-0164-0.

Yang L, Kemadjou JR, Zinsmeister C, Bauer M, Legradi J, Müller F, et al. Transcriptional profiling reveals barcode-like toxicogenomic responses in the zebrafish embryo. Genome Biol 2007;8:R227. http://dx.doi.org/10.1186/gb-2007-8-10-r227.

Yin Z, Jiang H, Swersen T, Rocha JB, Farina M, Aschner M. The methylmercury-L-cysteine conjugate is a substrate for the L-type large neutral amino acid transporter. J Neurochem 2008;107(4):1083–90. http://dx.doi.org/10.1111/j.1471-4159.2008.05683.x.

Yuan Y, Atchison WD. Action of methylmercury on GABA (A) receptor-mediated inhibitory synaptic transmission is primarily responsible for its early stimulatory effects on hippocampal CA1 excitatory synaptic transmission. J Pharmacol Exp Ther 1997;282(1):64–73.

Yuan Y, Otero-Montañez JK, Yao A, Herden CJ, Sirois JE, Atchison WD. Inward rectifying and voltage-gated outward potassium channels exhibit low sensitivity to methylmercury. Neurotoxicology 2005;26:439–54. http://dx.doi.org/10.1016/j.neuro.2005.03.005.

Zaiontz C. www.real-statistics.com, last accessed: November 9; 2014.

Zemolin APP, Meinerz DF, de Paula MT, Mariano DOC, Rocha JBT, Pereira AB, et al. Evidences for a role of glutathione peroxidase 4 (GPx4) in methylmercury induced neurotoxicity *in vivo*. Toxicology 2012;302:60–7. http://dx.doi.org/10.1016/j.tox.2012.07.013.